Article ID: 1000-324X(2016)08-0890-07 **DOI:** 10.15541/jim20150662

Luminescent and Cytotoxic Characteristics of an Ellipsoidal and Microsized Europium (Eu)-doped Hydroxyapatite

MA Ming[1], LU Wei-Peng[1], CAO Xiao-Feng[1], MAO Ke-Ya[2], GUO Yan-Chuan[1]

(1. Key Laboratory of Photochemical Conversion and Optoelectronic Material, Technical Institute of Physics and Chemistry, Chinese Academy of Sciences, Beijing 100190, China; 2. The General Hospital of People's Liberation Army (301 Hospital), Beijing 100853, China)

Abstract: A novel europium (Eu^{3+})-doped hydroxyapatite microspheres (Eu-HApMs) was successfully prepared *via* the calcium carbonate template and ion exchange process. The physicochemical, luminescent and cytotoxic properties of the prepared Eu-HApMs powders were investigated by the Scanning Electron Microscope (SEM), X-ray Diffraction (XRD), Inductively Coupled Plasma (ICP), and MTT assays *in vitro*. Results showed that Eu-HApMs particles exhibited an ellipsoidal morphology with diameters of about 2.5 μm and lengths of about 7 μm with a hedgehog-like surface. Besides, the pure hexagonal phase of hydroxyapatite with high crystallinity of Eu-HApMs and successful doping of Eu^{3+} ions into HApMs were revealed. The present study showed that the Eu-HApMs powders actually displayed red fluorescence under ultraviolet (UV) irradiation. It was evident that the $^5D_0 \rightarrow {}^7F_{1\text{-}4}$ transitions of Eu (III) ions played a key role in the photoluminescence (PL) activity. Finally, the MTT assay results revealed the continuous proliferation and no morphological change of MC3T3-E1 cells co-cultured with the extracts of Eu-HApMs powders and the calculated relative growth rate (RGR) indicating the cytotoxicity grade at level 1.

Key words: hydroxyapatite; biomaterials; europium-doped; ellipsoidal; fluorescence

Hydroxyapatite (HAp, $Ca_{10}(PO_4)_6(OH)_2$ has been considered as the molecular model to the mineral component of bones and tissues in human for decades, and was widely studied and commercially used in the fields of the reconstruction of damaged bone and teeth due to its biocompatible and non-inflammatory properties[1-3]. So far, many methods have been applied for the synthesis of HAp with different morphologies, including nano/micro-sized needles[4], rods[5], ribbons[6], plates[7], and spheres[8-9] and so on. Among these materials, the controlled production of spherical HAp particles with higher flowability still was needed to be extensively investigated since such particles were essential for the synthesis of bone cements or bone defect filling implants delivered into the host bone. In fact, HAp existed as hexagonal crystal (space group P63/m)[10] and spherical HAp particles cannot be obtained by the monocrystal growth method. So far, several routines have been reported for the spherical HAp preparation, for instance, wet chemical precipitation[11], flame-synthesis[12], spray-drying[13], and emulsification[14], *et al*. However, some disadvantages were found for these current synthesis of spherical hydroxyapatite methods, such as uncontrollable sphere size, long time consuming and chemical contamination.

Europium (Eu (III)) doped HAp (Eu-HAp) particles have also been regarded as biocompatible with no cytotoxicity and non-inflammatory[15-16] and were explored for developing biomedical applications such as gene therapy vector[17], luminescent drug carrier[18] and bioimaging contrast[19] for years. By virtue of its special features of the electronic configurations [Xe] $4f^n$ (n=0–14) of Eu (III), the luminescent $^5D_0 \rightarrow {}^7F_{1\text{-}4}$ transitions of Eu-HAp were sharp, time discriminated, easily recognizable and little sensitive to the chemical environments[20]. Moreover, these luminescent transitions of Eu-HAp spanned both the visible and near-infrared ranges which made them an ideal fluorescent agent for *in vitro* and *in vivo* biological imagines. For example, Doat, *et al*[21] research showed that Eu^{3+} ion luminescence can be irritated under visible light, and had a stable luminescence with time for prolonged

Received date: 2015-12-31; **Modified date:** 2016-02-15
Foundation item: Program of International Science and Technology Corporation, China (2013DFA50920); Science and Technology of Beijing, China (Z131100005213007); National Natural Sciences Foundation of China (51372276)
Biography: MA Ming(1985–), male, PhD. E-mail: maming@mail.ipc.ac.cn
Corresponding author: GUO Yan-Chuan, professor. E-mail: yanchuanguo@mail.ipc.ac.cn

examination of living cells. Mondéjar, *et al*[22] found that Eu-HAp was easily internalized by transformed human umbilical vein endothelial cells. Yang, *et al*[18] investigated that the luminescent intensity of Eu-HAp correlated with the released amount of ibuprofen (IBU), which made the drug release process be easily tracked and monitored by change of the luminescence intensity. Han, *et al*[19] utilized the Eu (III) doped HAp to label Bel-7402 human liver cancer cells as fluorescent probe and found that the strong green and red fluorescence were observed with excitation of blue and green light respectively. Chen, *et al*[23] indicated that Eu-HAp nanorods had a potential application in photoluminescence imaging.

In this paper, we proposed a convenient method to synthesize the Eu-HAp microsized particles with high crystallinity and controlled ellipsoidal morphology under mild reaction conditions. The morphology, phase, composition, luminescent property and cytotoxicity of the samples were well characterized by means of SEM, XRD, ICP, photoluminescent (PL) spectra and 3-(4,5-dimethyl-2- thiazolyl)-2,5-diphenyl-2-H-tetrazolium bromide (MTT) assays respectively.

1 Materials and methods

1.1 Synthesis of ellipsoidal calcium carbonate microspheres (CCMs)

0.2 mol/L $CaCl_2$ (Beijing chemical works, China) stock solution was rapidly poured into an equal volume of 0.2 mol/L Na_2CO_3 (Beijing chemical works, China) solution at 0℃, and after intense agitation with a mechanical stirrer for up to 1 h, the precipitate was filtered off, washed with de-ionized water and CCMs was obtained.

1.2 Synthesis of Eu(III)-doped hydroxyapatite microspheres (HApMs)

A total of 5.5 g of $(NH_4)_2HPO_4$ (Beijing chemical works, China) was dissolved in 900 mL of de-ionized water and 100 mL $NH_3{\cdot}H_2O$ (Beijing chemical works, China) was used to modulate the pH of the solution up to 11.0. Then the above prepared ellipsoidal CCMs were added to this $(NH_4)_2HPO_4$ solution. The aqueous suspension was immersed in 100℃ oil bath for conversion to HApMs as long as 47 h.

After reaction, 2 g of $Eu(NO_3)_3$ (Sigma, USA) were dissolved in 20 mL deionized water and mixed with the resulted HApMs suspension as described above. The reaction was further progressed at 100℃ in oil bath for 7 h and then the suspension was vacuum filtered, de-ionized water washed and dried at 50℃ in an oven, finally, Eu-HApMs were obtained.

1.3 Characterization

Morphological investigations of the precipitated powders were carried out with an S-4800 scanning electron microscope (Hitachi, Japan). XRD patterns of the as-precipitated powders and sintered powders were obtained using a D8 Focus (Bruker, Germany) powder diffractometer in the range between $10° \leqslant 2\theta \leqslant 70°$ with Cu K_α radiation (λ = 0.15406 nm), with a step size of 0.02º every 0.1 s. The actual Eu^{3+} doping concentration of samples were examined by inductively coupled plasma (ICP) analysis with a Varian 710-OES (Varian, USA). Photoluminescence emission and photoluminescence excitation (PLE) spectra were measured by a F-4500 fluorescence spectrophotometer (Hitachi, Japan) equipped with a xenon lamp and a solid sample holder accessory at room temperature.

1.4 Cell viability test

The extracts of the Eu-HApMs were prepared according to the protocols of the International Standard ISO 10993-12: 2012: Biological evaluation of medical devices-part 12: sample preparation and reference materials[24]. Generally, 0.2 g of the Eu-HApMs powders were immersed into 1 mL α-MEM medium (Institute of Basic Medical Sciences, China Academy of Medical Science, Beijing, China) at 37℃ for 72 h, then the supernatants were filtered with the 0.22 μm disposable needle filter for the cell viability test. The cell morphologies were characterized by Inverted biologic microscope (Chongqing Photoelectric Instrument Co., Ltd., China).

Mouse embryo preosteoblast cells (MC3T3-E1) (Institute of Basic Medical Sciences, China Academy of Medical Science, Beijing, China) were cultured in an α-MEM medium supplemented with 10% fetal bovine serum (FBS) at 37℃ for 48 h, and used for cell viability tests. The cells were digested with 0.05% trypsogen and dispersed into the new α-MEM medium supplemented with 10% FBS. Then the cells were seeded in 96 well flat-bottom microassay plates at a concentration of 1.5×10^3~2.0×10^3 cells/mL and cultured for 24 h. After 24 h, the supernatant fluid were discarded and the extracts of the Eu-HApMs particles were added into wells at the concentration of 0.2 g/mL, and co-cultured with cells for 1, 3, 5 and 7 d. The α-MEM medium supplemented with 10% FBS was used as a negative control. The cell viability was quantified by the MTT assay and measured at 490 nm on a microplate reader (Multiskan Mk3, Thermo Scientific, USA).

$$RGR = \left(\frac{\text{Experiment group everage}}{\text{negative group average}} \right) \times 100\% \qquad (1)$$

The cell viabilities were calculated and evaluated ac-

cording to the relative growth rate (RGR) expressed in equation (1). And the grade of cytotoxicity was correlated with the RGR data regulated in the United States Pharmacopeial Convention (Table 1)[25].

1.5 Statistical analysis

In this study, all experiments were done in quintuplicate and measurements repeated at least three times. The results were expressed as mean±standard deviation and statistically analyzed with one-way ANOVA method (software SPSS 20, SPSS Inc., USA). $P<0.05$ and $P<0.01$ were regarded as significant difference and extremely significant difference, respectively.

2 Results and discussion

2.1 Morphologies of CCMs, HApMs and Eu-HApMs

Fig. 1(a) showed typical SEM images of ellipsoidal CCMs particles. We could see that ellipsoid-like CCMs structures having a smooth surface with diameters of about 2.5 μm and lengths of about 7 μm were obtained. Fig. 1(b-d) showed typical SEM micrographs of ellipsoidal HApMs and Eu-HApMs which had similar sizes to those of the CCMs. The replacement of CO_3^{2-} by anions of PO_4^{3-}, the substitution of Ca(II) by cations of Eu(III), and the Eu(III) substitution time did not significantly change the morphologies and sizes of the CCMs, and the sizes kept constant throughout the whole reaction time (Fig. 1(c) and Fig. 1(d)). However, the CCMs surfaces became coarse and Hedgehog-like as the PO_4^{3-} source was directly poured into the CCMs suspension. The inset in Fig. 1(b) showed that needle shaped structures appeared on their surfaces. Accordingly, it can be deduced that the transformation of CCMs to HApMs was primarily *via* a dissolution-precipitation mechanism. As the CCMs particles were treated in $(NH_4)_2HPO_4$ solution at high temperature and pH conditions, Ca^{2+} could immediately react with PO_4^{3+} to form HApMs due to the lower thermodynamic free energy of hydroxyapatite than that of calcium carbonate.

Table 1 Correlation between RGR and grade of cytotoxicity

Relative growth rate/%	Grade of cytotoxicity	Cytotoxicity
⩾100	0	No
75–99	1	No
50–74	2	Analyzed with the cell morphology
5–49	3	Yes
1–24	4	Yes
0	5	Yes

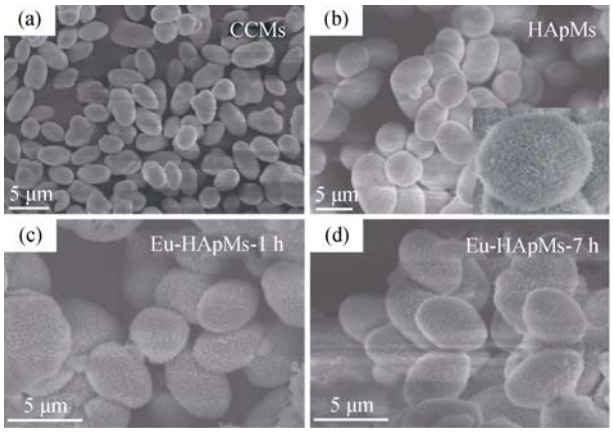

Fig. 1 SEM images of CCMs (a), HApMs (b) and Eu-HApMs (c: 1 h; d: 7 h)

As hydroxyapatite existed as hexagonal crystal, it would grow along the *c*-axis direction and form a Hedgehog-like morphology with needle shaped structure on its surface.

2.2 Phases of the samples

XRD patterns of the as-prepared CCMs, HApMs, Eu-HApMs and the transformation process of CCMs to HApMs were presented in Fig. 2 and Fig. 3. As shown in Fig. 2(a) and Fig. 2(b), the XRD pattern of the ellipsoidal CCMs was indexed to the well-crystallized rhombohedral calcite phase of calcium carbonate (JCPDS 47- 1743)[26], and the XRD pattern of the HAPMs was indexed to the hexagonal phase of hydroxyapatite (JCPDS 09-0432)[27]. Calcite is the most thermodynamically stable phase of calcium carbonate in the water[28]. In this work, calcium carbonate was synthesized in a lower temperature conditions and the low temperature was vital for the formation of calcite. Fig. 3 show the transformation process of CCMs to HAPMs. The peak intensity of calcium carbonate decreased quickly and largely as the CCMs particles were poured into the $(NH_4)_2HPO_4$ solution after 1 h, and complete replacement of PO_4^{3-} for CO_3^{2-} ions took place at or above 32 h. As the solubility product constant of hydroxyapatite (K_{sp}= 6.31×10^{-118})[29] was lower than that of calcium carbonate (K_{sp}=3.8×10^{-9})[30], the PO_4^{3-} would replace the CO_3^{2-} ions and preferentially combine with the Ca^{2+} ions to form the thermodynamically existed phase of hydroxyapatite at higher pH. The splitting and sharper of the typical planes (211), (112), (300), (202) belonging to hydroxyapatite indicated an improved crystalline structure of HApMs, in accordance with the needle shaped structure observed on its surface (Fig. 1(b) inset). The incorporation of Eu (III) ions in the crystal lattice of HApMs did not change the XRD patterns of the hexagonal phase of hydroxyapatite, and no additional crystallized phase could be detected.

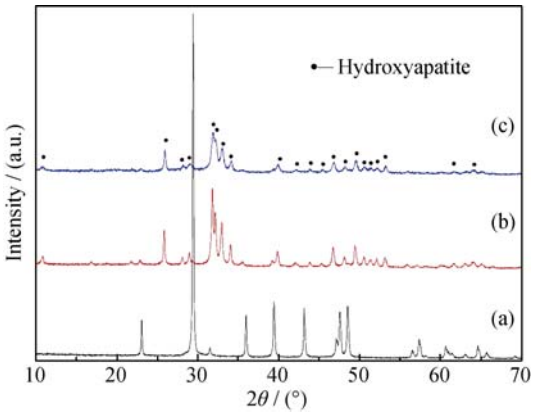

Fig. 2　XRD patterns of CCMs (a), HApMs (b) and Eu-HApMs (c)

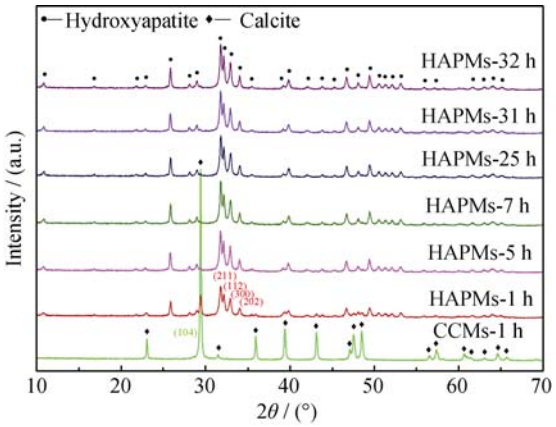

Fig. 3　XRD patterns of the transformation process of CCMs to HAPMs

The results showed that Eu (III) ions were successfully doped into the crystal lattice of HApMs. XRD pattern of Eu-HApMs (Fig. 2(c)) revealed a single phase of hydroxyapatite.

2.3　Ions release

In order to quantitatively determine the ion concentration changes of Ca^{2+} and Eu^{3+}, continuous sampling and the inductively coupled plasma (ICP) method was applied. Fig. 4 presented the amount of metal ions concentration changed during the doping period. It can be also clearly seen that the ions-doping process took place quickly. The doping process would reach an equilibrium point at 10 min as long as the HApMs powders were poured into the Eu^{3+} solution. Theoretical molar ratio of Ca: Eu was 10:1, and the final molar ratio was 10:1.21, indicating that the partial Ca^{2+} ions were successfully substituted and doped by Eu^{3+} ions. In fact, the ionic radii of the Eu^{3+} ions (94.7 pm) was smaller than that of Ca^{2+} ions (100 pm), and resulted in greater charge density and a high affinity of Eu^{3+} ions for Ca^{2+} sites.

2.4　Luminescence properties of Eu-HApMs

As shown in Fig. 5 (inset), the Eu-HApMs showed red luminescence under UV irradiation (365 nm). The PL properties of the sample were further characterized by the PL emission and excitation spectra. In the excitation

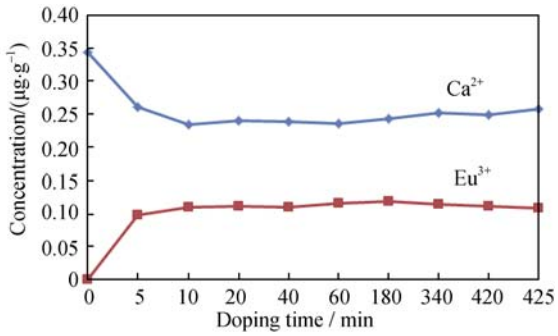

Fig. 4　ICP results of the ion-doping process

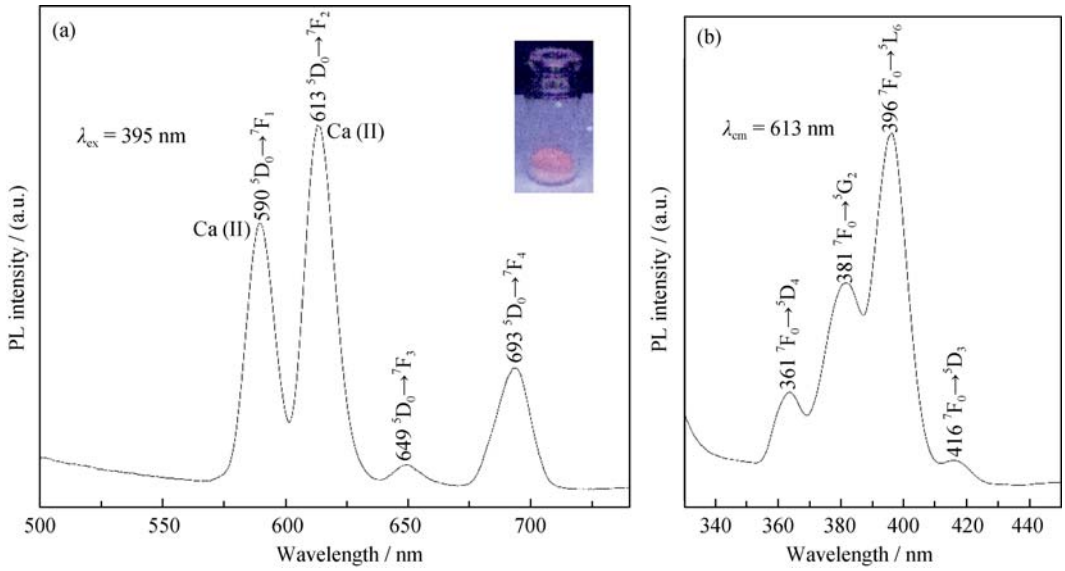

Fig. 5　Emission (a) and exciation (b) spectra of the ions-doped HAPMs
Inset is the corresponding photograph under ultraviolet (365 nm) irradiation

spectra monitored by the Eu^{3+} $^5D_0$-$^7F_2$ transition at 613 nm (Fig. 5(b)), peaks may arise from the direct excitation of the Eu^{3+} ground state into higher levels in the $4f^6$ configuration, which can be assigned to $^7F_0\rightarrow{}^5D_4$ (361 nm), $^7F_0\rightarrow{}^5G_2$ (381 nm), $^7F_0\rightarrow{}^5L_6$ (396 nm), $^7F_0\rightarrow{}^5D_3$ (416 nm), respectively[31-32]. In the emission spectra upon excitation at 395 nm, the characteristic transition lines of Eu^{3+} could be detected (Fig. 5(a)). The response from the Eu^{3+} ions in the powder corresponded to the typical $^5D_0\rightarrow{}^7F_J$ emissions and the four main characteristic peaks from $^5D_0\rightarrow{}^7F_1$ (590 nm), $^5D_0\rightarrow{}^7F_2$ (613 nm), $^5D_0\rightarrow{}^7F_3$ (649 nm), and $^5D_0\rightarrow{}^7F_4$ (693 nm) were predominant in the emission spectra.

In the crystal structure of apatite (space group P63/m), it permitted a wide range of cation and anion substitutions which would be introduced in the process of preparation. In particular two Ca^{2+} positions had distinct steorochemistry; the first type of site Ca(I) was of C_3 symmetry surrounded by nine oxygen atoms and the second type of site Ca(II) was of C_s symmetry surrounded by six oxygen ions and one OH^- ion[33]. Previous studies have shown that the Eu^{3+} ions predominantly occupied the Ca(II) site, and Eu^{3+} located in the Ca(I) position would completely migrated to Ca(II) position as the sample was thermally heated. In our experiment, the reaction temperature was 100℃ and the Eu^{3+} ions substituted Ca^{2+} through an ion-exchange process. And from our PL emission spectra, it can be seen that the Eu^{3+} ions located at the Ca(II) site with a higher local symmetry indicated by the relative intensity of the $^5D_0\rightarrow{}^7F_1$ (590 nm) and $^5D_0\rightarrow{}^7F_2$ (613 nm) transitions[34]. What's more, the PL luminescence results would also indicate the ions-doped HAPMs with a high crystallinity (Fig. 3(c)).

2.5 Cytotoxicity

Mitochondrial redox activity of the preosteoblast MC3T3-E1 cells in the extracts of Eu-HApMs was evaluated by reduction of MTT to formazan by mitochondrial succinate dehydrogenase which played a vital role in both oxidative phosphorylation and the tricarboxylic acid cycle. The higher the concentration of formazan was, the more active the MC3T3-E1 cells proliferated. Fig. 6(a) showed the MC3T3-E1 cells co-cultured with the extracts of Eu-HApMs powders for different culture times. It was notably that the cells were not disturbed by the extracts of Eu-HApMs powders, maintaining a healthy morphology, good adhesion and continuous proliferation. And the MTT values increased consecutively throughout the whole incubation period of 1, 3, 5, and 7 d (Fig. 6(b)), denoting that the cell proliferation was not affected after the long-time of Eu-HApMs exposure. As shown in Fig. 6(b), no significant change in cell viability was detected between the extracts of Eu-HApMs and the cell culture medium (contrast) at the beginning of culture time of 1 and 3 d, and the differences between these two samples became statistically significant (P<0.01) after prolonged incubation (5 d and 7 d). However, the calculated RGR results showed that the cytotoxicity grade was level 1 and confirmed that the Eu-HApMs powders were non-cytotoxic (Table 2).

Table 2 Results of the cytotoxicity test

Date/d	OD ($\bar{x}\pm s$)	RGR/%	Grade
1	0.165±0.044	132.48	0
3	0.819±0.044	110.05	0
5	1.376±0.091	79.90	1
7	1.531±0.050	89.54	1

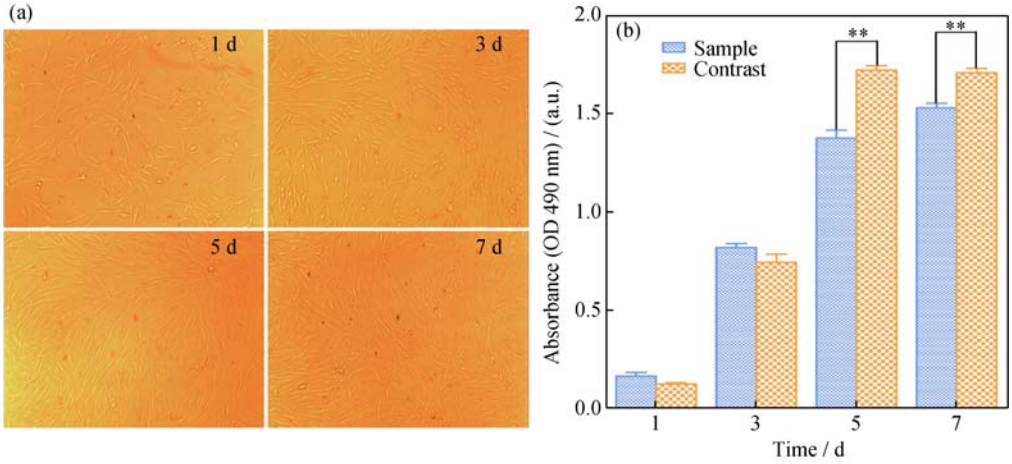

Fig. 6 (a) The MC3T3-E1 cells co-cultured with the extracts of Eu-HApMs powders for different culture time; (b) MTT results for tested Eu-HApMs for different culture time

*P<0.05, **P<0.01

3 Conclusions

In summary, a novel carbonate assisted process was proposed to synthesize an ellipsoidal Eu-HApMs particle under mild reaction conditions. The as-prepared Eu-HApMs powdrs were of high crystallinity. The morphologies of the as-prepared samples were ellipsoidal with a diameter of about 2.5 μm and a length of about 7 μm. The Eu^{3+} ions had no effects on the morphologies and crystalline structure of the final products. The as-made Eu-HApMs powders showed red luminescence under UV irradiation and exhibited four sharp emission peaks at $^5D_0 \rightarrow {}^7F_1$ (590 nm), $^5D_0 \rightarrow {}^7F_2$ (613 nm), $^5D_0 \rightarrow {}^7F_3$ (649 nm), and $^5D_0 \rightarrow {}^7F_4$ (693 nm) upon excitation at 395 nm. The *in vitro* MTT assay results showed that the cytotoxicity grade was level 1. In conclusion, the lack of Eu-HApMs powder' cytotoxicity held potential uses as a novel biomaterial with fluorescence in biomedical applications.

References:

[1] DOROZHKIN S V. Calcium orthophosphate bioceramics. *Ceramics International*, 2015, **41(10):** 13913–13966.

[2] DURACCIO D, MUSSANO F, FAGA M. Biomaterials for dental implants: current and future trends. *Journal of Materials Science*, 2015, **50(14):** 4779–4812.

[3] DUTTA S R , PASSI D, SINGH P, *et al*. Ceramic and non-ceramic hydroxyapatite as a bone graft material: a brief review. *Irish Journal of Medical Science*, 2015, **184(1):** 101–106.

[4] LIAO J G, LIU Q. Synthesis of nano-hydroxyapatite by microwave process and its characterization. *Rare Metal Materials and Engineering*, 2014, **43(7):** 1779–1782.

[5] ZHANG W, CHAI Y, XU X, *et al*. Rod-shaped hydroxyapatite with mesoporous structure as drug carriers for proteins. *Applied Surface Science*, 2014, **322:** 71–77.

[6] SUGANTHI R V, GIRIJA E K, NARAYANA KALKURA S, *et al*. Self-assembled right handed helical ribbons of the bone mineral hydroxyapatite. *Journal of Materials Science: Materials in Medicine*, 2009, **20(1):** 131–136.

[7] GIMENO-FABRA M, HILD F, DUNNE P W, *et al*. Continuous synthesis of dispersant-coated hydroxyapatite plates. *CrystEngComm*, 2015, **17(32):** 6175–6182.

[8] LI Z, WEN T, SU Y, *et al*. Hollow hydroxyapatite spheres fabrication with three-dimensional hydrogel template. *CrystEngComm*, 2014, **16(20):** 4202–4209.

[9] WEI X, KATHRYN G, ALMUT S, *et al*. Synthesis and release of trace elements from hollow and porous hydroxyapatite spheres. *Nanotechnology*, 2011, **22(30):** 305610.

[10] KAY M I, YOUNG R A, POSNER A S. Crystal structure of hydroxyapatite. *Nature*, 1964, **204(4963):** 1050–1052.

[11] LUO P, NIEH T G. Preparing hydroxyapatite powders with controlled morphology. *Biomaterials*, 1996, **17(20):** 1959–1964.

[12] WIDIYASTUTI, SETIAWAN A, SETYAWAN H, *et al*. Diffusion flame synthesis of hydroxyapatite nanoparticles using urea assisted precursor solution. *AIP Conference Proceedings*, 2011, **1415(1):** 152–154.

[13] CHOW L C, SUN L, HOCKEY B. Properties of nanostructured hydroxyapatite prepared by a spray drying technique. *Journal of Research of the National Institute of Standards and Technology*, 2004, **109(6):** 543–551.

[14] PRADEESH T S, SUNNY M C, VARMA H K, *et al*. Preparation of microstructured hydroxyapatite microspheres using oil in water emulsions. *Bulletin of Materials Science*, 2005, **28(5):** 383–390.

[15] POPA C, CIOBANU C, ICONARU S, *et al*. Systematic investigation and *in vitro* biocompatibility studies on mesoporous europium doped hydroxyapatite. *Central European Journal of Chemistry*, 2014, **12(10):** 1032–1046.

[16] HUI J, ZHANG X, ZHANG Z, *et al*. Fluoridated HAp:Ln^{3+} (Ln = Eu or Tb) nanoparticles for cell-imaging. *Nanoscale*, 2012, **4(22):** 6967–6970.

[17] HUANG S, ZHU J, ZHOU K. Effects of Eu^{3+} ions on the morphology and luminescence properties of hydroxyapatite nanoparticles synthesized by one-step hydrothermal method. *Materials Research Bulletin*, 2012, **47(1):** 24–28.

[18] YANG P, QUAN Z, LI C, *et al*. Bioactive, luminescent and mesoporous europium-doped hydroxyapatite as a drug carrier. *Biomaterials*, 2008, **29(32):** 4341–4347.

[19] HAN Y, WANG X, LI S. Biocompatible europium doped hydroxyapatite nanoparticles as a biological fluorescent probe. *Curr. Nanosci.*, 2010, **6:** 178.

[20] VICENTINI G, ZINNER L B, ZUKERMAN-SCHPECTOR J, *et al*. Luminescence and structure of europium compounds. *Coordination Chemistry Reviews*, 2000, **196(1):** 353–382.

[21] DOAT A, PELL F, GARDANT N, *et al*. Synthesis of luminescent bioapatite nanoparticles for utilization as a biological probe. *Journal of Solid State Chemistry*, 2004, **177(4/5):** 1179–1187.

[22] MONDÉJAR S P, KOVTUN A, EPPLE M. Lanthanide-doped calcium phosphate nanoparticles with high internal crystallinity and with a shell of DNA as fluorescent probes in cell experiments. *Journal of Materials Chemistry*, 2007**. 17(39):** 4153–4159.

[23] CHEN F, HUANG P, ZHU Y J, *et al*. Multifunctional Eu^{3+}/Gd^{3+}

dual-doped calcium phosphate vesicle-like nanospheres for sustained drug release and imaging. *Biomaterials*, 2012, **33(27):** 6447–6455.

[24] Biological Evaluation of Medical Devices-part 12: Sample Preparation and Reference Materials. International Organization for Standardization. ISO 10993–12: 2012.

[25] USP XXII, NF XVII. Toxicity Calssification in US Pharmacopeia. I. United States Pharmacopeial Convection. 1990**:** 2069.

[26] PHAM MINH D, TRAN N D, NZIHOU A, *et al*. One-step synthesis of calcium hydroxyapatite from calcium carbonate and orthophosphoric acid under moderate conditions. *Industrial & Engineering Chemistry Research*, 2013, **52(4):** 1439–1447.

[27] FARZADI A, BAKHSHI F, SOLATI-HASHJIN M, *et al*. Magnesium incorporated hydroxyapatite: Synthesis and structural properties characterization. *Ceramics International*, 2014, **40(4):** 6021–6029.

[28] QI R J, ZHU Y J. Microwave-assisted synthesis of calcium carbonate (vaterite) of various morphologies in water-ethylene glycol mixed solvents. *The Journal of Physical Chemistry B*, 2006, **110(16):** 8302–8306.

[29] LU X, LENG Y. Theoretical analysis of calcium phosphate precipitation in simulated body fluid. *Biomaterials*, 2005, **26(10):** 1097–1108.

[30] DONNET M, BOWEN P, LEMAıˆTRE J. A thermodynamic solution model for calcium carbonate: Towards an understanding of multi-equilibria precipitation pathways. *Journal of Colloid and Interface Science*, 2009, **340(2):** 218–224.

[31] YANG C, YANG P P, WANG W X, *et al*. Synthesis and characterization of Eu-doped hydroxyapatite through a microwave assisted microemulsion process. *Solid State Sciences*, 2009, **11(11):** 1923–1928.

[32] HUANG S, ZHU J, ZHOU K. Effects of Eu^{3+} ions on the morphology and luminescence properties of hydroxyapatite nanoparticles synthesized by one-step hydrothermal method. *Materials Research Bulletin*, 2012, **47(1):** 24–28.

[33] GRAEVE O A, KANAKALA R, MADADI A, *et al*. Luminescence variations in hydroxyapatites doped with Eu^{2+} and Eu^{3+} ions. *Biomaterials*, 2010, **31(15):** 4259–4267.

[34] MARTIN P, CARLOT G, CHEVARIER A, *et al*. Mechanisms involved in thermal diffusion of rare earth elements in apatite. *Journal of Nuclear Materials*, 1999, **275(3):** 268–276.

微米级椭球形掺铕羟基磷灰石的发光和细胞毒性研究

马 铭[1], 卢伟鹏[1], 曹霄峰[1], 毛克亚[2], 郭燕川[1]

(1. 中国科学院 理化技术研究所, 光化学转化与功能材料重点实验室, 北京 100190; 2. 解放军总医院(301 医院), 北京 100853)

摘 要: 利用碳酸钙模板和离子交换过程成功制备了一种新型掺铕羟基磷灰石微球。通过扫描电子显微镜(SEM)、X 射线衍射(XRD)、感应耦合等离子体(ICP)、光致发光谱和体外 MTT 实验对微球物化性能、发光性和细胞毒性进行了表征。研究结果显示: 掺铕羟基磷灰石微球呈椭球形, 直径约为 2.5 μm, 长度约为 7 μm, 并具有刺猬状表面; 在晶体结构上与纯相六方羟基磷灰石相同, 具有高结晶性; 铕离子成功进入羟基磷灰石晶相。同时, 研究还表明该掺铕羟基磷灰石颗粒在紫外光激发下显示出红色荧光。光致发光光谱表明铕离子的 $^5D_0 \rightarrow {}^7F_{1\text{-}4}$ 跃迁明显在光致发光活性中具有重要作用。体外细胞毒性实验结果显示: MC3T3-E1 小鼠胚胎骨细胞在掺铕羟基磷灰石浸提液中能够持续增殖, 没有细胞形态上的变化, 并且细胞相对增值率计算结果表明该掺铕羟基磷灰石细胞毒性等级为 1 级。

关 键 词: 羟基磷灰石; 生物材料; 铕掺杂; 椭球形; 荧光性

中图分类号: TQ174 **文献标识码:** A